

Effects of Different Phonon Scattering Factors on the Heat Transport Properties of Graphene Ribbons

Junjie Chen* and Lingyu Meng

Cite This: *ACS Omega* 2022, 7, 20186–20194

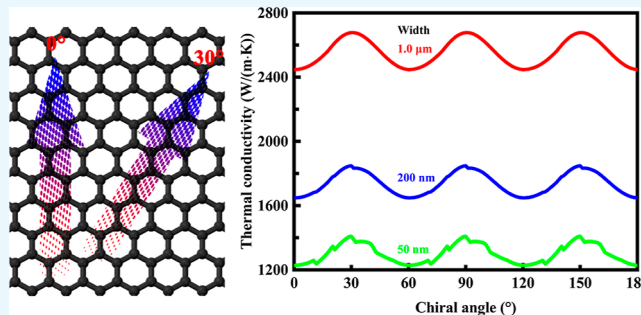
Read Online

ACCESS |

Metrics & More

Article Recommendations

ABSTRACT: Understanding the effect of phonon scattering is of primary significance in the study of the thermal transport properties of graphene. While phonon scattering negatively affects the thermal conductivity, the exact effect of microscopic phonon scattering is still poorly understood when full phonon dispersions are taken into account. The heat transport properties of graphene ribbons were investigated theoretically by taking into account different polarization branches with different frequencies in order to understand the physical mechanism of the thermal transport phenomenon at the nanoscale. The effects of grain size, chiral angle, Grüneisen anharmonicity parameter, specularly parameter, and mass-fluctuation-scattering parameter were evaluated, taking into account of the restrictions imposed by boundary, Umklapp, and isotope scattering mechanisms. The contribution from each phonon branch was estimated, and the anisotropic coefficients were determined accordingly. The results indicated that the graphene ribbons are very efficient at conducting heat in all the cases studied. All the acoustical branches contribute significantly to the heat transport properties, and the temperature strongly affects the relative contribution of the phonon branches. The lattice thermal conductivity varies periodically with the chiral angle. The maximum thermal conductivity is achieved in the zigzag direction, and the minimum thermal conductivity is obtained in the armchair direction. The lattice thermal conductivity and anisotropic coefficient depend heavily upon the roughness of the edges and the width of the ribbons. The specularly parameter and mass-fluctuation-scattering parameter significantly affect the lattice thermal conductivity, and the effect arising from isotope scattering is significant in the context of natural isotopic abundance. The dependence of the Grüneisen anharmonicity parameter on phonon branches must be taken into account when making predictions. The results have significant implications for the understanding of the relations between phonon scattering and thermal properties.



1. INTRODUCTION

Graphene is a two-dimensional form of crystalline carbon.^{1,2} Graphene is the simplest example of a two-dimensional crystal and commonly modified with various functional groups.^{3,4} Graphene ribbons are a special category of graphene, with a high aspect ratio.^{5,6} In this regard, the two-dimensional material does bear similarity to carbon nanotubes.^{7,8} Various techniques such as microscope lithography and organic synthesis have been developed to produce minuscule amounts of graphene ribbons.^{9,10} Microscopic quantities of the two-dimensional material can be produced by plasma etching methods^{11,12} or by chemical vapor deposition techniques.^{13,14} Graphene ribbons produced by these techniques and methods are typically characterized by several coupled layers with a disordered structure of the edges.

Graphene ribbons possess unique physical properties, for example, exceptional electrical properties. Unlike carbon nanotubes, which can be semiconducting, semi-metallic, or metallic depending upon the diameter and chirality,^{15,16} graphene ribbons would exhibit remarkable electrical properties,

which are significantly affected by the ribbon width and edge configuration.^{17,18} For example, graphene ribbons with a width of greater than around 10 nm are semi-metallic or metallic conductors, whereas graphene ribbons with a width of less than around 10 nanometers are semiconductors.^{19,20} The edge configurations, for example, a zigzag or armchair arrangement, greatly affect the electron mobility,^{21,22} and the edges may behave like semiconductors. Such zigzag and armchair arrangements are analogous to those defined in the context of carbon nanotubes.^{23,24} The bandgap would still be zero in a zigzag arrangement and would be non-zero in an armchair arrangement.

Received: April 2, 2022

Accepted: May 18, 2022

Published: May 27, 2022



The term “conductivity” may refer to thermal or electrical transport properties. Analogies might be made between thermal and electrical conductivity. This is because heat and electron transfer could be closely related to each other. Additionally, conduction is the most significant means of heat and electron transfer within a solid. Ballistic conduction is not limited to electrons²⁵ but can also apply to phonons.²⁶ A good electrical conductor would conduct heat well. The thermal properties of graphene ribbons are also governed by their width and their edge configurations and functionalization,^{27,28} which do have a certain similarity to the electrical properties.^{17,18} The question arises as to whether or not graphene ribbons can be superconductors, conductors, or insulators in terms of lattice thermal conductivity, depending upon microscopic phonon scattering. Accordingly, the spectrum of thermal conductivity might be determined, which can provide more than just the magnitude of the thermal conductivity, for example, the mechanisms of phonon transport in the nanostructured material.

In graphene ribbons, heat is transported by phonons, which have a wide variation in frequency. The scale of the physical system may be comparable to the phonon mean free path or even the phonon wavelength.^{27,28} This clearly necessitates an understanding of the physical mechanism of the thermal transport phenomenon at the nanoscale. This equality in length scales raises fundamental conceptual problems concerning nanoscale thermal transport,^{29,30} among which is the effects of different phonon scattering factors on the heat transport properties of graphene ribbons. This fundamental problem remains to be resolved.^{31,32} While phonon scattering negatively affects the lattice thermal conductivity, the exact effect of microscopic phonon scattering is still poorly understood when taking account of full phonon dispersions and the mechanisms involved remain obscure.

The present study relates to the effects of different phonon scattering factors on the thermal properties of a two-dimensional crystal, namely, graphene ribbons, especially when the characteristic length is smaller than the mean free path. The effects of grain size, chiral angle, Grüneisen anharmonicity parameter, specular parameter, and mass-fluctuation-scattering parameter on the lattice thermal conductivity were evaluated based upon the solutions of the Boltzmann transport equation to better understand the mechanisms responsible for phonon scattering. The contribution from each phonon branch was estimated, and the anisotropic coefficients were determined accordingly. The objective of this study is to understand the relationship between phonon scattering and thermal properties. Particular emphasis is placed on the effects of different phonon scattering factors on the heat transport properties of graphene ribbons.

2. METHODS

2.1. Full Phonon Dispersions. The computations are performed with full phonon dispersions in order to predict the thermal conductivity accurately. The phonon dispersion relationship has been determined using Raman spectroscopy^{33,34} and from the spectrum of inelastic X-ray scattering.^{35,36} The fourth-nearest neighbor force constant method^{37–40} is reparameterized to account for the relationship between the phonon modes. Specifically, the non-diagonal force constant for the second-nearest neighbor interaction is taken into account;^{41,42} the in-of-plane and out-of-plane tangential force constants are adjusted.^{43,44} The longitudinal acoustic, transverse

acoustic, zone-boundary acoustic, and zone-boundary optical branches are taken into account over the first Brillouin zone. The effects of the other two optical branches are not taken into account due to their negligible contribution to the lattice thermal conductivity. The phonon dispersion is anisotropic, and therefore, the group velocity of the phonons depends heavily upon the direction of phonon angular momentum.^{33–36} More specifically, the phonons have high levels of propagation velocities in the armchair direction in the longitudinal acoustic and zone-boundary optical branches and in the zig-zag direction in the transverse acoustic and zone-boundary acoustic branches. The structure of the graphene ribbon described in terms of the chiral angle is illustrated schematically in Figure 1. Carbon

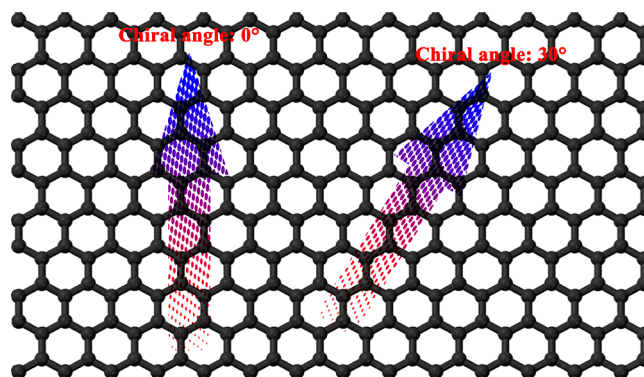


Figure 1. Schematic representation of the structure of the graphene ribbon described in terms of the chiral angle. Carbon atoms are represented by dark grey spheres. The chiral angle is defined as the angle between the chiral vector and the zigzag direction.

atoms are represented by dark gray spheres. For purposes of the description herein, the chiral angle is defined as the angle between the chiral vector and the zigzag direction.

2.2. Boltzmann Transport Equation. The Boltzmann transport equation for the spatially nonuniform phonon distribution can be written as follows

$$\left(\frac{\partial f}{\partial t}\right)_{\text{drift}} + \left(\frac{\partial f}{\partial t}\right)_{\text{scattering}} = 0 \quad (1)$$

in which f is the distribution function and t is the time.

The relaxation time approximation is used. The scattering term can be written as

$$\left(\frac{\partial f}{\partial t}\right)_{\text{scattering}} = -\frac{f - f_0}{\tau} \quad (2)$$

in which f and f_0 represent the perturbed and unperturbed distribution functions, respectively, and τ is the relaxation time.

The unperturbed distribution function can be written as

$$f_0 = (e^{\hbar\omega/k_B T} - 1)^{-1} \quad (3)$$

in which \hbar is the reduced Planck's constant, k_B is the Boltzmann constant, and T is absolute temperature. The above formula is often referred to as the Bose–Einstein distribution function.

The difference between the perturbed and unperturbed distribution functions can be written as

$$f - f_0 = -\tau(\vec{v}_g \cdot \nabla T) \frac{\partial f_0}{\partial T} \quad (4)$$

$$\vec{v}_g = \frac{\partial \omega}{\partial \vec{q}} \quad (5)$$

in which \vec{v}_g is the phonon group velocity, ω is the angular frequency, and \vec{q} is the phonon wave vector.

Thermal transport in the two-dimensional crystal is usually considered to be governed by the three-phonon scattering process. There are two possible scattering processes. For the case (i), two incoming phonons with wave vectors \vec{q} and \vec{q}' create one outgoing phonon with a wave vector \vec{q}''

$$\vec{q} + \vec{q}' = \vec{b}_i + \vec{q}'', \quad i = 1, 2, 3 \quad (6)$$

$$\omega + \omega' = \omega'' \quad (7)$$

in which \vec{b}_i is a vector of the reciprocal lattice.

For the case (ii), one incoming phonon with a wave vector \vec{q} decays into two outgoing phonons with wave vectors \vec{q}' and \vec{q}''

$$\vec{q} + \vec{b}_i = \vec{q}' + \vec{q}'', \quad i = 4, 5, 6 \quad (8)$$

$$\omega = \omega' + \omega'' \quad (9)$$

2.3. Boundary Scattering. The phonon transport is partially diffusive, and the boundary scattering can be evaluated by the specularly parameter, which represents the fraction of phonons specularly reflected at the boundary.^{45,46} The specularly parameter typically depends upon the phonon wavelengths and edge roughness.^{47,48} For the boundary scattering process, the relaxation time related to a phonon in the state (s, \vec{q}) can be written as follows

$$\frac{1}{\tau_B(s, \vec{q})} = \frac{v_s(\omega_s)}{d} \frac{1-p}{1+p} \quad (10)$$

in which $\tau_B(s, \vec{q})$ is the relaxation time related to phonon-boundary scattering, s is the phonon polarization branch, v is the phonon velocity, d is the width of the ribbon, and p is the specularly parameter.

The specularly parameter can be computed as follows

$$p = \exp(-4\eta^2 q^2 \cos^2 \theta) \quad (11)$$

in which η is the root-mean-square roughness and θ is the angle of incidence.

2.4. Umklapp Scattering. For the Umklapp scattering process, the relaxation time related to a phonon in the state (s, \vec{q}) can be written as follows^{49,50}

$$\frac{1}{\tau_U(s, \vec{q})} = \frac{\hbar \gamma_s^2(\vec{q})}{\bar{M} T_D v_s^2(\vec{q})} \omega_s^2(\vec{q}) T e^{-\frac{T_D}{3T}} \quad (12)$$

in which $\tau_U(s, \vec{q})$ is the relaxation time related to Umklapp scattering, \hbar is the reduced Planck's constant, $\gamma_s(\vec{q})$ is the mode-dependent Grüneisen anharmonicity parameter, \bar{M} is the average atomic mass, T_D is the Debye temperature, and T is the temperature. The above expression has been derived from the problems of lattice thermal conductivity related to carbon nanotubes,⁵¹ graphene flakes,⁵² and graphene.^{53,54} The Debye temperature is given by

$$T_D^2 = \frac{5\hbar^2 \int \omega^2 g_s(\omega) d\omega}{3k_B^2 \int g_s(\omega) d\omega} \quad (13)$$

in which k_B is the Boltzmann constant and $g_s(\omega)$ is the phonon density of states per each branch.

The two-dimensional phonon density of states per each branch is given by

$$g_s(\omega) = \frac{1}{4\pi^2} \sum_{q_x(s,\omega)} \sum_{q_y(s,\omega,q_x)} \frac{\Delta q_x}{|v_y(q_x, q_y, s)|} \quad (14)$$

$$v_y = \frac{\partial \omega}{\partial q_y} \quad (15)$$

in which q_x and q_y are the components of the two-dimensional phonon wave vector, v_y is the y -component of the phonon group velocity, and Δq_x is the interval between two neighboring q_x points.

The mode-dependent Grüneisen anharmonicity parameter can be written as follows

$$\gamma_s(\vec{q}) = -\frac{a}{2\omega_s(\vec{q})} \frac{d\omega_s(\vec{q})}{da} \quad (16)$$

in which a is the lattice constant.

The Grüneisen anharmonicity parameter is given as follows^{52–56}

$$\frac{\gamma_{LA}(\vec{q})}{\gamma_{TA}(\vec{q})} \approx 3 \quad (17)$$

$$\gamma_{LA}(\vec{q}) \approx 2 \quad (18)$$

$$\gamma_{TA}(\vec{q}) \approx \text{constant} \quad (19)$$

$$\gamma_{ZA}(\vec{q}) \approx -1.5 \quad (20)$$

$$\gamma_{ZO}(\vec{q}) \approx -1.5 \quad (21)$$

in which the subscript LA denotes the longitudinal acoustic branch, the subscript TA denotes the transverse acoustic branch, the subscript ZA denotes the zone-boundary acoustic branch, and the subscript ZO denotes the zone-boundary optical branch.

2.5. Isotope Scattering. For the isotope scattering process, the relaxation time related to a phonon in the state (s, \vec{q}) can be written as follows

$$\frac{1}{\tau_I(s, \vec{q})} = \frac{\Gamma V_0}{12\omega^2 g(\omega)} \quad (22)$$

in which $\tau_I(s, \vec{q})$ is the relaxation time related to isotope scattering, Γ is the mass-fluctuation-scattering parameter, V_0 is the atomic volume, and $g(\omega)$ is the total phonon density of states.

The total phonon density of states can be obtained by summation of the contributions over all phonon branches

$$g(\omega) = \sum_s g_s(\omega) \quad (23)$$

The mass-fluctuation-scattering parameter of the isotopic composition is given by

$$\Gamma = \sum_i f_i \left(1 - \frac{M_i}{\bar{M}}\right)^2 = \frac{c(1-c)}{(12-c)^2} \quad (24)$$

in which f_i is the fraction of component i , M_i is the atomic mass of component i , and c is the fraction of carbon-13. The naturally occurring ratio of carbon-13 to carbon-12 is around 1.11:98.89.

2.6. Lattice Thermal Conductivity Model. All the scattering processes described above are taken into account. The combined relaxation time can be approximated as follows

$$\frac{1}{\tau(s, \vec{q})} = \frac{1}{\tau_B(s, \vec{q})} + \frac{1}{\tau_U(s, \vec{q})} + \frac{1}{\tau_I(s, \vec{q})} \quad (25)$$

The total thermal conductivity tensor can be obtained by summing over all the phonon branches described above

$$k_{ij}(T) = \frac{1}{\delta} \sum_{s, \vec{q}} v_i(s, \vec{q}) v_j(s, \vec{q}) \frac{\hbar \omega(s, \vec{q})}{\tau(s, \vec{q})} \frac{\partial N_0(\omega(s, \vec{q}))}{\partial T} \quad (26)$$

in which k_{ij} is the total thermal conductivity tensor, $v_i(s, \vec{q})$ and $v_j(s, \vec{q})$ are the components of the phonon group velocity vector, and N_0 is the number of phonons.

The components of the phonon group velocity vector are given by

$$v_i(s, \vec{q}) = \frac{\partial \omega(s, \vec{q})}{\partial q_i} \quad (27)$$

$$v_j(s, \vec{q}) = \frac{\partial \omega(s, \vec{q})}{\partial q_j} \quad (28)$$

The thermal conductivity in a particular direction can be written as follows

$$k_{\hat{i}}(T) = \sum_{ij} \hat{i}_i k_{ij}(T) \hat{i}_j \quad (29)$$

in which \hat{i} is the unit vector in a particular direction.

The thermal conductivity vector can be turned into physically scalar by projecting the phonon velocity vector onto the direction of thermal transport

$$v_{\hat{i}}(\vec{q}) = \vec{v}(\vec{q}) \cdot \hat{i} = \|\vec{v}(\vec{q})\| \cos \theta_{\hat{i}} \quad (30)$$

in which $\theta_{\hat{i}}$ is the angle formed by the phonon velocity vector and the unit vector in the direction of thermal transport.

The anisotropic coefficient is defined as follows

$$\alpha = \frac{k_{\text{zigzag}}}{k_{\text{armchair}}} - 1 \quad (31)$$

in which α is the anisotropic coefficient. The anisotropic coefficient is positive and takes into account the lattice thermal conductivity in different directions.

3. RESULTS AND DISCUSSION

3.1. Effect of Grain Size. Much effort has been placed on understanding the thermal properties of two-dimensional crystals,^{27,28} especially when the characteristic length is comparable to the mean free path. For graphene, the mean free path is around 780 nm at room temperature.^{29,30,48} The effect of ribbon width on the thermal conductivity at different temperatures is investigated to better understand the mechanism responsible for phonon boundary scattering. The specularly parameter is defined by eq 11 to facilitate ease of understanding and compare the effect of phonon boundary scattering.

The results obtained for the thermal conductivity are presented in Figure 2. The graphene ribbon varies considerably in width. The width of the two-dimensional crystal is 500 nm, 2 μm , and 5 μm , respectively. The specularly parameter is 0.9, and

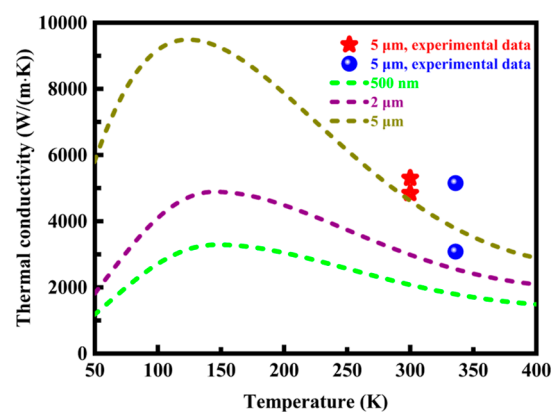


Figure 2. Lattice thermal conductivity as a function of temperature for graphene ribbons with different widths. The specularly parameter is 0.9, and the Grüneisen anharmonicity parameter is mode-dependent. The experimental data obtained for a width of 5 μm are presented for comparison.

the Grüneisen anharmonicity parameter is mode-dependent. The specularly parameter is estimated based on reported literature values.^{57,58} The experimental data obtained for a width of 5 μm available in the literature^{57,58} are also presented for comparison. The theoretical results agree with the experimental data. The thermal conductivity increases with the width of the ribbon due to the reduced probability of diffusive scattering of the phonons at the boundary. In all the cases studied here, there is at most a three-fold increase in the thermal conductivity. When the width of the ribbon, for example, 500 nm, is less than the mean free path, the thermal conductivity is still much higher than that of a highly conductive metal. The precise value will vary depending upon the temperature. At lower temperatures, the thermal conductivity associated with the crystal lattice structure increases with temperature. At moderate and higher temperatures, the thermal conductivity is inversely proportional to temperature due to the increased degree of Umklapp scattering.

3.2. Contribution from Different Phonon Branches.

The contribution from different phonon branches is estimated for the graphene ribbon by applying a mode-dependent Grüneisen anharmonicity parameter to the problem of nanoscale phonon transport. The thermal conductivity per each phonon branch is shown in Figure 3. The graphene ribbon with a width of 5 μm is taken as an example to illustrate, with which phonon scattering dominates over grain boundary scattering. The specularly parameter is 0.9, and the Grüneisen anharmonicity parameter is mode-dependent. The Grüneisen anharmonicity parameter remains constant for each phonon branch of the vibrational spectrum so that the contribution from each branch can be easily determined.

The lattice thermal conductivity depends upon the vibrational modes of the crystal lattice structure, as shown in Figure 3. At room temperature, the transverse acoustic branch has the largest contribution. At lower temperatures, the zone-boundary acoustic branch has the largest contribution. In all the cases studied here, the acoustical branches contribute significantly, whereas the contribution of the zone-boundary optical branch to the thermal conductivity is very small. With reference to Figure 3, phonons in the acoustical branches dominate the nanoscale thermal transport in the crystal lattice structure, since the acoustic phonons have a greater distribution of phonon velocities.^{59,60} The group velocity of the optical

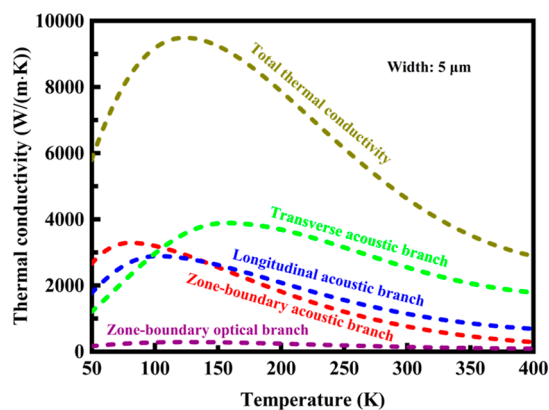


Figure 3. Lattice thermal conductivity as a function of temperature per each phonon branch. The width of the ribbon is $5 \mu\text{m}$. The specular parameter is 0.9, and the Grüneisen anharmonicity parameter is mode-dependent.

branches is low,^{59,60} and as a result, the contribution is small. The contribution from each phonon branch varies considerably with temperature, especially at lower temperatures. The temperature greatly affects the relative contribution of the phonon branches.

3.3. Effect of Chiral Angle. The effect of chiral angle on the thermal conductivity of the two-dimensional crystal with different widths is illustrated in Figure 4. The specular

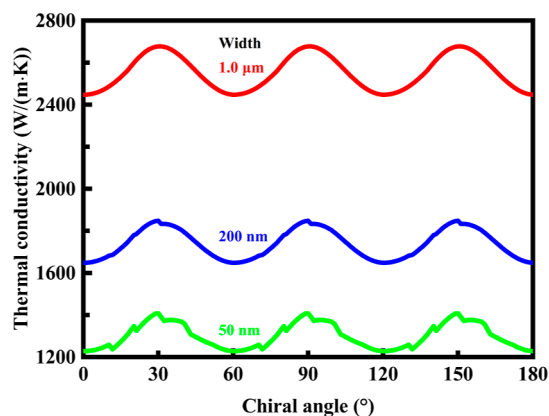


Figure 4. Effect of chiral angle on the lattice thermal conductivity of the two-dimensional crystal with different widths. The specular parameter is 0.9, and the Grüneisen anharmonicity parameter is mode-dependent.

parameter is 0.9, and the Grüneisen anharmonicity parameter is mode-dependent. When the chiral angle is 0° , the edge has an armchair configuration. When the chiral angle is 30° , the edge has a zigzag configuration.

The thermal conductivity varies periodically with the chiral angle, as shown in Figure 4. The thermal conductivity is periodic with period 60° . More specifically, the thermal conductivity is a periodic function, which repeats on intervals of 60° . The graphene ribbon with a width of $1.0 \mu\text{m}$ provides the ability to conduct heat highly efficiently while enabling the thermal conductivity to remain in the range of about 2440 K to about 2680 K. In all the cases studied here, the maximum thermal conductivity is achieved at a chiral angle of 30° , at which the edge has a zigzag configuration. In contrast, the minimum thermal conductivity is obtained at a chiral angle of 0° , at which

the edge has an armchair configuration. Therefore, the thermal conductivity depends upon the direction of thermal transport. For wider graphene ribbons, the transverse acoustic branch significantly contributes to the thermal conductivity, leading to larger, yet gentle changes of the thermal conductivity with respect to the chiral angle, as shown in Figure 4. In this case, the dimensions are much larger than the phonon mean free path, and therefore, Umklapp phonon–phonon scattering dominates over grain boundary scattering. For narrower graphene ribbons for which the dimensions are smaller than the mean free path, phonon-boundary scattering dominates over Umklapp scattering. Accordingly, the thermal conductivity decreases significantly and varies irregularly in a periodic manner with the chiral angle.

3.4. Anisotropic Coefficients. The effect of edge roughness on the thermal conductivity and anisotropic coefficient of the graphene ribbons with different widths in the armchair direction is illustrated in Figure 5 and in Figure 6, respectively.

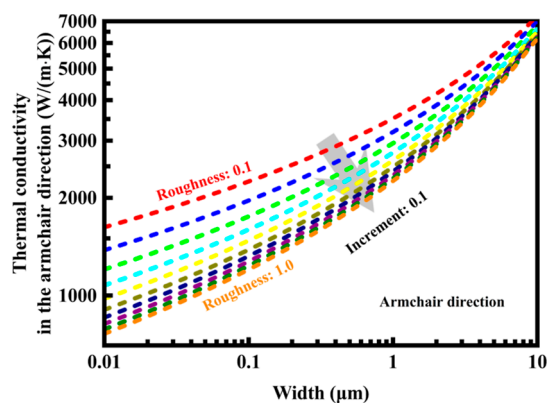


Figure 5. Effect of edge roughness on the lattice thermal conductivity of the two-dimensional crystal with different widths in the armchair direction. The root-mean-square roughness of the edges gradually increases from 0.1 to 1.0 with an increment of 0.1. The Grüneisen anharmonicity parameter is mode-dependent.

The root-mean-square roughness of the edges gradually increases from 0.1 to 1.0 with an increment of 0.1. In addition, the Grüneisen anharmonicity parameter is mode-dependent.

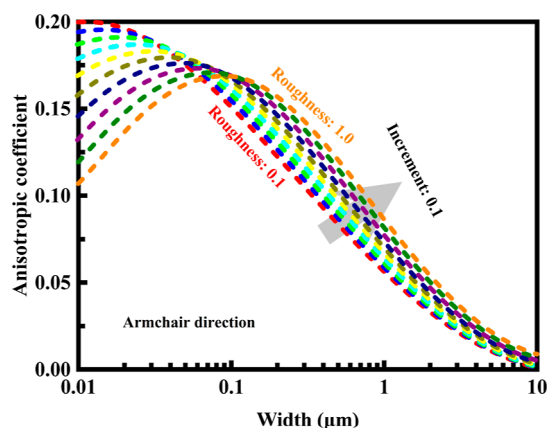


Figure 6. Effect of edge roughness on the anisotropic coefficient of the two-dimensional crystal with different widths in the armchair direction. The root-mean-square roughness of the edges gradually increases from 0.1 to 1.0 with an increment of 0.1. The Grüneisen anharmonicity parameter is mode-dependent.

The thermal conductivity and anisotropic coefficient depend heavily upon the roughness of the edges and the width of the ribbons, as shown in Figure 5. The thermal conductivity in the armchair direction increases with decreasing the roughness of the edges and with increasing the width of the ribbons. Advantageously, the edges should be smooth enough to allow the desired level of thermal conductivity in the armchair direction. The ribbons should also be wide enough to achieve the desired thermal conductivity level in the armchair direction despite the existing limitations in producing graphene ribbons of any significant length. While a comparatively high level of thermal conductivity is necessary or desirable, graphene ribbons have yet to be made in practical macro-scale lengths. The maximum anisotropic coefficient will depend upon both the roughness of the edges and the width of the ribbons, as shown in Figure 6. The graphene ribbons vary significantly in anisotropic coefficient with the width of the ribbons. For narrower graphene ribbons, smooth edges have the disadvantage of larger anisotropic coefficients. In contrast, wider graphene ribbons would be difficult or even impossible to achieve isotropic thermal properties. In this case, the anisotropic coefficient increases with the roughness of the edges.

3.5. Effect of Grüneisen Anharmonicity Parameter.

The effect of Grüneisen anharmonicity parameter on the thermal conductivity is illustrated in Figure 7. The thermal

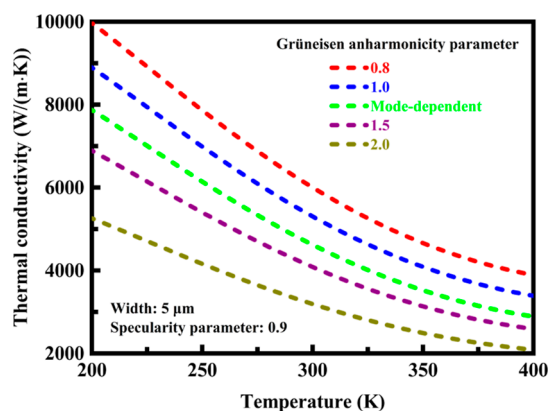


Figure 7. Effect of the Grüneisen anharmonicity parameter on the lattice thermal conductivity at different temperatures. The width of the ribbon is $5 \mu\text{m}$, and the specularity parameter is 0.9.

conductivity is plotted against temperature. The graphene ribbon varies considerably in the Grüneisen anharmonicity parameter. Specifically, the Grüneisen anharmonicity parameter is 0.8, 1.0, 1.5, 2.0, or mode-dependent. The width of the ribbon is $5 \mu\text{m}$, and the specularity parameter is 0.9. The temperature varies from 200 to 400 K. The Grüneisen anharmonicity parameter is determined empirically. In the theory of the nature of conventional semiconductors, the Grüneisen anharmonicity parameter is physically scalar and independent of any temperature or phonon mode.⁵⁴ However, there is a noticeable difference in the Grüneisen anharmonicity parameter between graphite,⁶¹ graphene,^{54,62} and carbon nanotubes.^{63–66} In the present study, the Grüneisen anharmonicity parameter is mode-dependent, with mode dependence based on all phonon branches computed via density functional theory and the basic theory of crystal lattice dynamics.⁵⁶ The Grüneisen anharmonicity parameter can be up to 2.0 for graphene^{54,62} and as low as 1.06 for graphite,^{61,66} which are larger than the theoretical limit of 0.8.⁵⁶ However, it has been demonstrated that the Grüneisen

anharmonicity parameter decreases with increasing temperature.^{67,68} Therefore, the results of lattice thermal conductivity are presented with a wide range of the Grüneisen anharmonicity parameter.

The thermal conductivity at room temperature varies from about $3200 \text{ W}/(\text{mK})$ with a Grüneisen anharmonicity parameter of 2.0 to about $6000 \text{ W}/(\text{mK})$ with a Grüneisen anharmonicity parameter of 0.8, as shown in Figure 7. When the Grüneisen anharmonicity parameter is mode-dependent, the thermal conductivity at room temperature is about $4600 \text{ W}/(\text{mK})$. Therefore, the Grüneisen anharmonicity parameter has a considerable effect on the thermal conductivity. For the Umklapp scattering process, the relaxation time is inversely proportional to the Grüneisen anharmonicity parameter squared, as defined by eq 12. In all the cases studied here, there is at most a two-fold increase in the thermal conductivity, since the presence of other scattering mechanisms reduces the dependency induced by the Grüneisen anharmonicity parameter. The theoretical results predicted with the mode-dependent Grüneisen anharmonicity parameter are consistent with the experimental data available in the literature,^{57,58} as shown in Figure 2. Consequently, the dependence of the Grüneisen anharmonicity parameter on phonon branches must be taken into account when making predictions.

3.6. Effect of Specularity Parameter and Mass-Fluctuation-Scattering Parameter. The specularity parameter typically depends upon the edge roughness.^{47,48} The effect of the specularity parameter on the thermal conductivity is investigated for three different cases. The theoretical results are presented in Figure 8, in which the thermal conductivity is

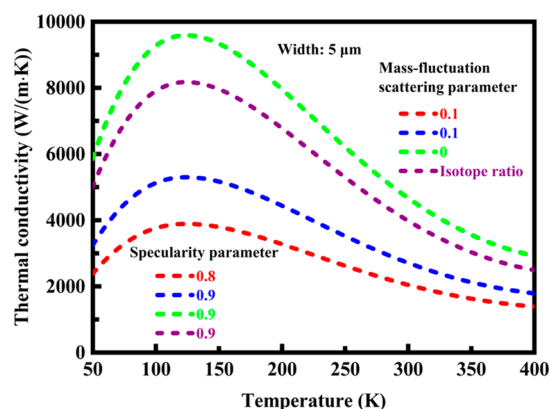


Figure 8. Lattice thermal conductivity as a function of temperature for different cases of specularity parameter and mass-fluctuation-scattering parameter. The width of the ribbon is $5 \mu\text{m}$, and the mass-fluctuation-scattering parameter is 0, 0.1, and the isotope ratio, respectively. The specularity parameter is 0.8 and 0.9, respectively.

plotted against temperature for different cases of the specularity parameter and mass-fluctuation-scattering parameter. The specularity parameter is 0.8 and 0.9, respectively. In addition, the width of the ribbon is $5 \mu\text{m}$, and mass-fluctuation-scattering parameters are 0 and 0.1, respectively.

The specularity parameter significantly affects the thermal conductivity of graphene ribbons. This effect becomes more pronounced at lower temperatures, as shown in Figure 8. The mass-fluctuation-scattering parameter also strongly affects the thermal conductivity, especially at lower temperatures. Natural-abundance stable-isotopic analysis of graphene is used, and the stable isotopes are carbon-12 and carbon-13. Isotope ratio mass

spectrometry is a specialized branch of mass spectrometry utilizing the relative abundance of isotopes,^{69,70} and the methodology allows for the precise measurement of mixtures of naturally occurring isotopes. The natural isotopic abundance of carbon-13 and carbon-12 is 1.109 and 98.891%. Therefore, the naturally occurring ratio of carbon-13 to carbon-12 is about 1.11:98.89, as stated previously. Differences in mass between different isotopes may reduce the ability to conduct heat. The results presented in Figure 8 indicate that the reduction ratio of thermal conductivity is very high, and therefore, the effect arising from isotope scattering is significant in the context of natural isotopic abundance.

4. CONCLUSIONS

The heat transport properties of graphene ribbons at different temperatures were investigated theoretically by taking into account full phonon dispersions. The effects of different phonon scattering factors, such as grain size, chiral angle, Grüneisen anharmonicity parameter, specular parameter, and mass-fluctuation-scattering parameter, on the lattice thermal conductivity were evaluated based upon the numerical solutions of the Boltzmann transport equation in order to understand the thermal transport phenomena occurring in the nanostructured material. The contribution from each phonon branch was estimated by applying a mode-dependent Grüneisen anharmonicity parameter, and the anisotropic coefficients were determined accordingly.

- The results indicated that the lattice thermal conductivity is significantly higher than that of highly conductive metals in all the cases studied. All the acoustical branches contribute significantly to the heat transport properties, whereas the contribution of the zone-boundary optical branch to the lattice thermal conductivity is very small. The contribution from each phonon branch varies considerably with temperature, especially at lower temperatures.
- For narrower graphene ribbons, the crystal structure displays anisotropic thermal transport. The thermal conductivity varies periodically with the chiral angle. The thermal conductivity is periodic with period 60°. The maximum thermal conductivity of the two-dimensional crystal is achieved at a chiral angle of 30°, at which the edge has a zigzag configuration. The minimum thermal conductivity is obtained at a chiral angle of 0°, at which the edge has an armchair configuration. The thermal conductivity and anisotropic coefficient depend heavily upon the roughness of the edges and the width of the ribbons.
- The Grüneisen anharmonicity parameter has a considerable effect on the thermal conductivity. The dependence of the Grüneisen anharmonicity parameter on phonon branches must be taken into account when making predictions. The specular parameter and mass-fluctuation-scattering parameter significantly affect the lattice thermal conductivity, and the effects become more pronounced at lower temperatures. The effect arising from isotope scattering is significant in the context of natural isotopic abundance.

AUTHOR INFORMATION

Corresponding Author

Junjie Chen – Department of Energy and Power Engineering, School of Mechanical and Power Engineering, Henan Polytechnic University, Jiaozuo, Henan 454000, P. R. China; orcid.org/0000-0001-8348-4896; Email: cjjmmm@163.com

Author

Lingyu Meng – Department of Energy and Power Engineering, School of Mechanical and Power Engineering, Henan Polytechnic University, Jiaozuo, Henan 454000, P. R. China

Complete contact information is available at:

<https://pubs.acs.org/10.1021/acsomega.2c02039>

Notes

The authors declare no competing financial interest.

ACKNOWLEDGMENTS

This work was supported by the Science Foundation for Outstanding Young Teachers in Institutions of Higher Education in Henan Province (no. 2019GGJS054).

REFERENCES

- (1) Geim, A. K.; Novoselov, K. S. The rise of graphene. *Nat. Mater.* **2007**, *6*, 183–191.
- (2) Geim, A. K. Graphene: Status and prospects. *Science* **2009**, *324*, 1530–1534.
- (3) Georgakilas, V.; Otyepka, M.; Bourlinos, A. B.; Chandra, V.; Kim, N.; Kemp, K. C.; Hobza, P.; Zboril, R.; Kim, K. S. Functionalization of graphene: Covalent and non-covalent approaches, derivatives and applications. *Chem. Rev.* **2012**, *112*, 6156–6214.
- (4) Quintana, M.; Vazquez, E.; Prato, M. Organic functionalization of graphene in dispersions. *Acc. Chem. Res.* **2013**, *46*, 138–148.
- (5) Shinde, P. V.; Tripathi, A.; Thapa, R.; Rout, C. S. Nanoribbons of 2D materials: A review on emerging trends, recent developments and future perspectives. *Coord. Chem. Rev.* **2022**, *453*, 214335.
- (6) Zeng, W.; Wu, J. Open-shell graphene fragments. *Chem* **2021**, *7*, 358–386.
- (7) Kosynkin, D. V.; Higginbotham, A. L.; Sinititskii, A.; Lomeda, J. R.; Dimiev, A.; Price, B. K.; Tour, J. M. Longitudinal unzipping of carbon nanotubes to form graphene nanoribbons. *Nature* **2009**, *458*, 872–876.
- (8) Kim, K.; Sussman, A.; Zettl, A. Graphene nanoribbons obtained by electrically unwrapping carbon nanotubes. *ACS Nano* **2010**, *4*, 1362–1366.
- (9) Han, M. Y.; Özyilmaz, B.; Zhang, Y.; Kim, P. Energy band-gap engineering of graphene nanoribbons. *Phys. Rev. Lett.* **2007**, *98*, 206805.
- (10) Tapasztó, L.; Dobrik, G.; Lambin, P.; Biró, L. P. Tailoring the atomic structure of graphene nanoribbons by scanning tunnelling microscope lithography. *Nat. Nanotechnol.* **2008**, *3*, 397–401.
- (11) Ma, L.; Wang, J.; Ding, F. Recent progress and challenges in graphene nanoribbon synthesis. *ChemPhysChem* **2013**, *14*, 47–54.
- (12) Jiao, L.; Zhang, L.; Wang, X.; Diankov, G.; Dai, H. Narrow graphene nanoribbons from carbon nanotubes. *Nature* **2009**, *458*, 877–880.
- (13) Terrones, M.; Botello-Méndez, A. R.; Campos-Delgado, J.; López-Urías, F.; Vega-Cantú, Y. I.; Rodríguez-Macías, F. J.; Elías, A. L.; Muñoz-Sandoval, E.; Cano-Márquez, A. G.; Charlier, J.-C.; Terrones, H. Graphene and graphite nanoribbons: Morphology, properties, synthesis, defects and applications. *Nano Today* **2010**, *5*, 351–372.
- (14) Bai, J.; Huang, Y. Fabrication and electrical properties of graphene nanoribbons. *Mater. Sci. Eng.* **2010**, *70*, 341–353.
- (15) Bernholc, J.; Brenner, D.; Nardelli, M. B.; Meunier, V.; Roland, C. Mechanical and electrical properties of nanotubes. *Annu. Rev. Mater. Res.* **2002**, *32*, 347–375.

- (16) Ilani, S.; McEuen, P. L. Electron transport in carbon nanotubes. *Annu. Rev. Condens. Matter Phys.* **2010**, *1*, 1–25.
- (17) Young, A. F.; Kim, P. Electronic transport in graphene heterostructures. *Annu. Rev. Condens. Matter Phys.* **2011**, *2*, 101–120.
- (18) Sangwan, V. K.; Hersam, M. C. Electronic transport in two-dimensional materials. *Annu. Rev. Phys. Chem.* **2018**, *69*, 299–325.
- (19) Wang, X.; Ouyang, Y.; Li, X.; Wang, H.; Guo, J.; Dai, H. Room-temperature all-semiconducting sub-10-nm graphene nanoribbon field-effect transistors. *Phys. Rev. Lett.* **2008**, *100*, 206803.
- (20) Li, X.; Wang, X.; Zhang, L.; Lee, S.; Dai, H. Chemically derived, ultrasmooth graphene nanoribbon semiconductors. *Science* **2008**, *319*, 1229–1232.
- (21) Nakada, K.; Fujita, M.; Dresselhaus, G.; Dresselhaus, M. S. Edge state in graphene ribbons: Nanometer size effect and edge shape dependence. *Phys. Rev. B: Condens. Matter Mater. Phys.* **1996**, *54*, 17954–17961.
- (22) Areshkin, D. A.; Gunlycke, D.; White, C. T. Ballistic transport in graphene nanostrips in the presence of disorder: Importance of edge effects. *Nano Lett.* **2007**, *7*, 204–210.
- (23) Lu, J.-Q.; Wu, J.; Duan, W.; Liu, F.; Zhu, B.-F.; Gu, B.-L. Metal-to-semiconductor transition in squashed armchair carbon nanotubes. *Phys. Rev. Lett.* **2003**, *90*, 156601.
- (24) Rocha, C. G.; Dargam, T. G.; Latgé, A. Electronic states in zigzag carbon nanotube quantum dots. *Phys. Rev. B: Condens. Matter Mater. Phys.* **2002**, *65*, 165431.
- (25) Du, X.; Skachko, I.; Barker, A.; Andrei, E. Y. Approaching ballistic transport in suspended graphene. *Nat. Nanotechnol.* **2008**, *3*, 491–495.
- (26) Saito, R.; Mizuno, M.; Dresselhaus, M. S. Ballistic and diffusive thermal conductivity of graphene. *Phys. Rev. Appl.* **2018**, *9*, 024017.
- (27) Pop, E.; Varshney, V.; Roy, A. K. Thermal properties of graphene: Fundamentals and applications. *MRS Bull.* **2012**, *37*, 1273–1281.
- (28) Balandin, A. A. Thermal properties of graphene and nanostructured carbon materials. *Nat. Mater.* **2011**, *10*, S69–S81.
- (29) Seol, J. H.; Jo, I.; Moore, A. L.; Lindsay, L.; Aitken, Z. H.; Pettes, M. T.; Li, X.; Yao, Z.; Huang, R.; Broido, D.; Mingo, N.; Ruoff, R. S.; Shi, L. Two-dimensional phonon transport in supported graphene. *Science* **2010**, *328*, 213–216.
- (30) Cahill, D. G.; Braun, P. V.; Chen, G.; Clarke, D. R.; Fan, S.; Goodson, K. E.; Keblinski, P.; King, W. P.; Mahan, G. D.; Majumdar, A.; Maris, H. J.; Phillpot, S. R.; Pop, E.; Shi, L. Nanoscale thermal transport. II. 2003–2012. *Appl. Phys. Rev.* **2014**, *1*, 011305.
- (31) Hooeboom-Pot, K. M.; Hernandez-Charpak, J. N.; Gu, X.; Frazer, T. D.; Anderson, E. H.; Chao, W.; Falcone, R. W.; Yang, R.; Murnane, M. M.; Kapteyn, H. C.; Nardi, D. A new regime of nanoscale thermal transport: Collective diffusion increases dissipation efficiency. *Proc. Natl. Acad. Sci. U.S.A.* **2015**, *112*, 4846–4851.
- (32) Cahill, D. G.; Ford, W. K.; Goodson, K. E.; Mahan, G. D.; Majumdar, A.; Maris, H. J.; Merlin, R.; Phillpot, S. R. Nanoscale thermal transport. *J. Appl. Phys.* **2003**, *93*, 793–818.
- (33) Samsonidze, G. G.; Saito, R.; Jorio, A.; Filho, A. G.; Grüneis, A.; Pimenta, M. A.; Dresselhaus, G.; Dresselhaus, M. S. Phonon trigonal warping effect in graphite and carbon nanotubes. *Phys. Rev. Lett.* **2003**, *90*, 027403.
- (34) Grüneis, A.; Saito, R.; Kimura, T.; Cañado, L. G.; Pimenta, M. A.; Jorio, A.; Filho, A. G. S.; Dresselhaus, G.; Dresselhaus, M. S. Determination of two-dimensional phonon dispersion relation of graphite by Raman spectroscopy. *Phys. Rev. B: Condens. Matter Mater. Phys.* **2002**, *65*, 155405.
- (35) Mohr, M.; Maultzsch, J.; Dobardžić, E.; Reich, S.; Milošević, I.; Damnjanović, M.; Bosak, A.; Krisch, M.; Thomsen, C. Phonon dispersion of graphite by inelastic x-ray scattering. *Phys. Rev. B: Condens. Matter Mater. Phys.* **2007**, *76*, 035439.
- (36) Maultzsch, J.; Reich, S.; Thomsen, C.; Reuquardt, H.; Ordejón, P. Phonon dispersion in graphite. *Phys. Rev. Lett.* **2004**, *92*, 075501.
- (37) Saito, R.; Dresselhaus, G.; Dresselhaus, M. S. *Physical Properties of Carbon Nanotubes*; Imperial College Press: London, United Kingdom, 1998; pp 163–182.
- (38) Aksamija, Z.; Knezevic, I. Lattice thermal conductivity of graphene nanoribbons: Anisotropy and edge roughness scattering. *Appl. Phys. Lett.* **2011**, *98*, 141919.
- (39) Al-Jishi, R.; Dresselhaus, G. Lattice-dynamical model for graphite. *Phys. Rev. B: Condens. Matter Mater. Phys.* **1982**, *26*, 4514–4522.
- (40) Jishi, R. A.; Venkataraman, L.; Dresselhaus, M. S.; Dresselhaus, G. Phonon modes in carbon nanotubes. *Chem. Phys. Lett.* **1993**, *209*, 77–82.
- (41) Wirtz, L.; Rubio, A. The phonon dispersion of graphite revisited. *Solid State Commun.* **2004**, *131*, 141–152.
- (42) Grüneis, A.; Attacalite, C.; Wirtz, L.; Shiozawa, H.; Saito, R.; Pichler, T.; Rubio, A. Tight-binding description of the quasiparticle dispersion of graphite and few-layer graphene. *Phys. Rev. B: Condens. Matter Mater. Phys.* **2008**, *78*, 205425.
- (43) Gartstein, Y. N. Vibrations of single-wall carbon nanotubes: Lattice models and low-frequency dispersion. *Phys. Lett. A* **2004**, *327*, 83–89.
- (44) Zimmermann, J.; Pavone, P.; Cuniberti, G. Vibrational modes and low-temperature thermal properties of graphene and carbon nanotubes: Minimal force-constant model. *Phys. Rev. B: Condens. Matter Mater. Phys.* **2008**, *78*, 045410.
- (45) Chen, G. Non-Fourier phonon heat conduction at the microscale and nanoscale. *Nat. Rev. Phys.* **2021**, *3*, S55–S69.
- (46) Zobiri, O.; Atia, A.; Arıcı, M. Mesoscale investigation of specularly parameter impact on heat transport in graphene nanoribbon. *Phys. E* **2022**, *139*, 115153.
- (47) Ravichandran, N. K.; Zhang, H.; Minnich, A. J. Spectrally resolved specular reflections of thermal phonons from atomically rough surfaces. *Phys. Rev. X* **2018**, *8*, 041004.
- (48) Nika, D. L.; Pokatilov, E. P.; Askerov, A. S.; Balandin, A. A. Phonon thermal conduction in graphene: Role of Umklapp and edge roughness scattering. *Phys. Rev. B: Condens. Matter Mater. Phys.* **2009**, *79*, 155413.
- (49) Morelli, D. T.; Heremans, J. P.; Slack, G. A. Estimation of the isotope effect on the lattice thermal conductivity of group IV and group III-V semiconductors. *Phys. Rev. B: Condens. Matter Mater. Phys.* **2002**, *66*, 195304.
- (50) Yu, X.-G.; Liang, X.-G. Effect of isotope on lattice thermal conductivity of lateral epitaxial overgrown GaN. *Diam. Relat. Mater.* **2007**, *16*, 1711–1715.
- (51) Cao, J. X.; Yan, X. H.; Xiao, Y.; Ding, J. W. Thermal conductivity of zigzag single-walled carbon nanotubes: Role of the umklapp process. *Phys. Rev. B: Condens. Matter Mater. Phys.* **2004**, *69*, 073407.
- (52) Nika, D. L.; Ghosh, S.; Pokatilov, E. P.; Balandin, A. A. Lattice thermal conductivity of graphene flakes: Comparison with bulk graphite. *Appl. Phys. Lett.* **2009**, *94*, 203103.
- (53) Kong, B. D.; Paul, S.; Nardelli, M. B.; Kim, K. W. First-principles analysis of lattice thermal conductivity in monolayer and bilayer graphene. *Phys. Rev. B: Condens. Matter Mater. Phys.* **2009**, *80*, 033406.
- (54) Klemens, P. G.; Pedraza, D. F. Thermal conductivity of graphite in the basal plane. *Carbon* **1994**, *32*, 735–741.
- (55) D'Souza, R.; Mukherjee, S. First-principles study of the electrical and lattice thermal transport in monolayer and bilayer graphene. *Phys. Rev. B* **2017**, *95*, 085435.
- (56) Mounet, N.; Marzari, N. First-principles determination of the structural, vibrational and thermodynamic properties of diamond, graphite, and derivatives. *Phys. Rev. B: Condens. Matter Mater. Phys.* **2005**, *71*, 205214.
- (57) Balandin, A. A.; Ghosh, S.; Bao, W.; Calizo, I.; Teweldebrhan, D.; Miao, F.; Lau, C. N. Superior thermal conductivity of single-layer graphene. *Nano Lett.* **2008**, *8*, 902–907.
- (58) Ghosh, S.; Calizo, I.; Teweldebrhan, D.; Pokatilov, E. P.; Nika, D. L.; Balandin, A. A.; Bao, W.; Miao, F.; Lau, C. N. Extremely high thermal conductivity of graphene: Prospects for thermal management applications in nanoelectronic circuits. *Appl. Phys. Lett.* **2008**, *92*, 151911.

(59) Ziman, J. M. *Electrons and Phonons: The theory of transport phenomena in solids*; Clarendon Press: Oxford, United Kingdom, 1960; pp 31–48.

(60) Pichanusakorn, P.; Bandaru, P. Nanostructured thermoelectrics. *Mater. Sci. Eng., R* **2010**, *67*, 19–63.

(61) Hanfland, M.; Beister, H.; Syassen, K. Graphite under pressure: Equation of state and first-order Raman modes. *Phys. Rev. B: Condens. Matter Mater. Phys.* **1989**, *39*, 12598–12603.

(62) Thomsen, C.; Reich, S.; Ordejón, P. Ab initio determination of the phonon deformation potentials of graphene. *Phys. Rev. B: Condens. Matter Mater. Phys.* **2002**, *65*, 073403.

(63) Reich, S.; Jantoljak, H.; Thomsen, C. Shear strain in carbon nanotubes under hydrostatic pressure. *Phys. Rev. B: Condens. Matter Mater. Phys.* **2000**, *61*, R13389.

(64) Popov, M.; Kyotani, M.; Nemanich, R. J.; Koga, Y. Superhard phase composed of single-wall carbon nanotubes. *Phys. Rev. B: Condens. Matter Mater. Phys.* **2002**, *65*, 033408.

(65) Schelling, P. K.; Keblinski, P. Thermal expansion of carbon structures. *Phys. Rev. B: Condens. Matter Mater. Phys.* **2003**, *68*, 035425.

(66) Popov, M.; Kyotani, M.; Koga, Y. Superhard phase of single wall carbon nanotube: comparison with fullerite C60 and diamond. *Diam. Relat. Mater.* **2003**, *12*, 833–839.

(67) Abdullaev, N. A. Grüneisen parameters for layered crystals. *Phys. Solid State* **2001**, *43*, 727–731.

(68) Abdullaev, N. A.; Suleimanov, R. A.; Aldzhanov, M. A.; Alieva, L. N. On the role played by bending vibrations in heat transfer in layered crystals. *Phys. Solid State* **2002**, *44*, 1859–1863.

(69) Chen, H.; Li, Y.; Jiang, W.; Xiong, Y. Determination of carbon isotopic composition of crocetane in sediments by heart-cutting two-dimensional gas chromatography-isotope ratio mass spectrometry. *J. Chromatogr. A* **2022**, *1666*, 462878.

(70) Brenna, J. T.; Corso, T. N.; Tobias, H. J.; Caimi, R. J. High-precision continuous-flow isotope ratio mass spectrometry. *Mass Spectrom. Rev.* **1997**, *16*, 227–258.